RSC Advances

PAPER

View Article Online
View Journal | View Issue

Cite this: *RSC Adv.*, 2022, **12**, 26476

g-C_3N_5-dots as fluorescence probes prepared by an alkali-assisted hydrothermal method for cell imaging†

Xiangwang Zeng,[a] Mengke Hou,[a] Pan Zhu,[a] Minyi Yuan,[a] Sitao Ouyang,[a] Qiujun Lu,[a] Chenxi Zhao,[a] Haiyan Wang, *[a] Fuyou Du,*[a] Guangsheng Zeng*[a] and Youyu Zhang *[b]

Received 26th June 2022
Accepted 18th August 2022

DOI: 10.1039/d2ra03934f

rsc.li/rsc-advances

Carbon nitride materials have become one of the highly explored carbon-based nanomaterials due to their unique properties. Herein, the novel graphitic carbon nitride quantum dots (g-C_3N_5-dots) were synthesized using an alkali-assisted hydrothermal method. The proposed strategy was simple, time-saving and the entire synthetic process only takes 60 min. And the prepared g-C_3N_5-dots showed excellent dispersion and good stability in water. What is more, the g-C_3N_5-dots displayed bright blue fluorescence with a high quantum yield of 12%. It was found that the g-C_3N_5-dots exhibited peroxidase-like activity, good biocompatibility and low cytotoxicity and can be successfully applied in cell imaging. The proposed method opens a new and efficient way for the preparation of fluorescent g-C_3N_5-dots and facilitates g-C_3N_5-dots for bioimaging and related biological sensing applications.

1 Introduction

Fluorescent nanomaterials have greatly attracted attention because of their excellent fluorescent performance and special small size effect.[1,2] In the development of fluorescent nanomaterials, semiconductor quantum dots (QDs), such as PbS QDs and CdTe QDs, usually have size-tunable and narrow emission spectra, high photostability, and resistance to metabolic degradation in bioapplications.[3–5] Although great success has been achieved on semiconductor QDs and rare earth ion doped nanoparticles, the heavy metals of semiconductor QDs caused high toxicity to the organism. Additionally, low biocompatibility limited the application of semiconductor QDs in biological systems. Therefore, it is very necessary to develop non-toxic or low toxic fluorescent nanomaterials instead of semiconductor QDs.

Recently, graphitic carbon nitrides (CN), as a type of carbon-based nanomaterials, have secured considerable interest due to their unique properties, such as low toxicity, fascinating electronic band structure, unique structural characteristics and being environment friendly.[6,7] Among these CN materials, g-C_3N_4 is the most extensively investigated photocatalyst due to its chemical stability and a tunable electronic structure. Currently available g-C_3N_4-based materials including layered g-C_3N_4 and composites based on g-C_3N_4 generally have been applied in many fields such as photocatalysis,[8–10] photodegradation,[11,12] antibacterial field,[13–16] sensors[17,18] and so on. However, the g-C_3N_4 is generally limited to the C/N ratio higher than 0.75 *i.e.* C_3N_4. The relatively low nitrogen content in the carbon framework suffer from low stability, further limiting their performance in various applications.[19] Recently, Vinu *et.al.* reported a novel carbon nitride with the more nitrogen content (with g-C_3N_5 stoichiometry ratio).[19,20] It was demonstrated that the g-C_3N_5 provided much better electronic properties than g-C_3N_4 with less nitrogen content.[21] And the novel g-C_3N_5 extended its absorption in visible region. It implies that the g-C_3N_5 has more excellent optical performances. On the other hand, the g-C_3N_5 had more surface functional groups (such as –NH_2 groups) largely improving the interaction between g-C_3N_5 and the guest species (*e.g.* biomolecules, biomarker).[22] It implies that the g-C_3N_5 has great potential in the field of biochemical analysis. In addition, the triazole structure also endowed g-C_3N_5 to be fluorescence, chemical stabilization and biocompatibility. From the above, the g-C_3N_5 is expected to use as a novel and ideal fluorescent material.

Although the bulk g-C_3N_5 exhibits great potential for optical application, there are still some problems need to be overcome before its practical application. Firstly, the strong interactions between g-C_3N_5 layers make it insoluble in water. Secondly, the g-C_3N_5 with the relatively low fluorescence quantum yields (FLQY) is sub-micrometer-sized. The large size of g-C_3N_5 limits

[a]*College of Biological and Chemical Engineering, Changsha University, Changsha, 410022, China. E-mail: wanghaiyan@ccsu.edu.cn; dufu2005@126.com; guangsheng_zeng@126.com; Fax: +86-731-84261382; Tel: +86-84261506*

[b]*Key Laboratory of Chemical Biology and Traditional Chinese Medicine Research (Ministry of Education), College of Chemistry and Chemical Engineering, Hunan Normal University, Changsha 410081, China. E-mail: zhangyy@hunnu.edu.cn*

† Electronic supplementary information (ESI) available. See https://doi.org/10.1039/d2ra03934f

its wide application in the biological fields. Compared with the bulk materials, the quantum dots (such as graphene quantum dots, graphene oxide quantum dots) with sizes less than 10 nm have excellent optical properties, better hydrophilicity and more suitable for biological applications.[23–25] Therefore, it will be interesting to develop effective routes for cutting bulk g-C_3N_5 into quantum dots-sized pieces *i.e.* g-C_3N_5 quantum dots (g-C_3N_5-dots), and the g-C_3N_5-dots will be promising candidate fluorescence materials for optical, biomedical, and cellular imaging areas.

It is noted that CN is a graphite-like layered material linked to planar amino groups in each layer and weak van der Waals force between the layers.[26,27] This special structure leads to the easy break of bonds between interlayers, while making it difficult to break the C–N bonds on the layers.[28] Therefore, it is very necessary to develop a simple and efficient method to prepare g-C_3N_5-dots. Herein, we reported the synthesis of g-C_3N_5-dots through a facile alkaline assisted-hydrothermal strategy using bulk g-C_3N_5 as precursor firstly. Compared with other reported methods, the proposed synthesis method of CN quantum dots was low-cost, fast and simple (Table S1).† And the entire synthetic process of g-C_3N_5-dots only required 60 min. The as-synthesized g-C_3N_5-dots exhibited high fluorescence (FL) with FLQY of 12%. Meanwhile, the g-C_3N_5-dots displayed peroxidase-like activity and well optical properties including acid resistance, alkaline resistance, salt stability, photo-stability, resistance to photo-bleaching. As satisfactory FL probes, the as-prepared g-C_3N_5-dots with good biocompatibility and low cytotoxicity were successfully applied in FL imaging of HeLa cells directly.

2 Experimental section

2.1 Materials

3-Amino-1,2,4-triazole, NaCl, HCl, NaOH, methylthiazolydiphenyltetrazolium bromide (MTT), quinine sulfate, ethyl acetate (EA), trichloromethane ($CHCl_3$) and dimethylsulfoxide (DMSO), *o*-phenylenediamine (OPD), and 3′,3′,5,5′-tetramethylbenzidine dihydrochloride (TMB·2HCl) were obtained from Shanghai Reagent (Shanghai, China). All other chemicals used in this work were of analytical grade. FLQY was determined using a previously published procedure by using quinine sulfate as a reference standard (FLQY = 54%). Millipore Milli-Q ultrapure water (Millipore, ≥18 M cm^{-1}, U.S.A) was used throughout the experiments.

2.2 Apparatus

Transmission electron microscope (TEM) images were collected from a JEM-2100 transmission electronic microscope (JEM, Japan). The ultraviolet-visible (UV-vis) spectra were obtained by a UV-2450 UV-vis spectrophotometer (Shimadzu Co., Japan). An F-7000 fluorescence spectrophotometer (Hitachi Co., Japan) was applied for the fluorescence analysis. Fourier transform infrared spectra (FT-IR) were recorded on a Nicolet Nexus 670 FT-IR spectroscope (Nicolet Instrument Co., USA). X-ray photoelectron spectroscopy (XPS) data was measured by a K-Alpha 1063 XPS (Thermo Fisher Co. U.K.) for analyzing structure information of g-C_3N_5-dots.

2.3 Preparation of bulk g-C_3N_5

The bulk g-C_3N_5 was prepared by direct thermal treatment of 3-amino-1,2,4-triazole. Briefly, 4 g 3-amino-1,2,4-triazole was put into an alumina crucible and then heated from the room temperature to 500 °C with a ramp rate of 13 °C min^{-1} in air. Finally, the deep yellow bulk g-C_3N_5 was obtained after cooling to room temperature and then grounded into fine powders in the agate mortar.

2.4 Preparation of g-C_3N_5-dots

The g-C_3N_5-dots were prepared by an alkali-assisted hydrothermal method. Typically, 0.03 g bulk g-C_3N_5 powder mixed with 0.3 g NaOH and 10 mL H_2O under stirring. Then the solution was transferred into a 25 mL Teflon lined stainless steel autoclave. Afterward, the sealed autoclave was heated to 180 °C in an electric oven and kept for 60 min. After naturally cooled to room temperature, the product was centrifuged at 8000 rpm for 5 min to remove the large size particles and dialyzed against water through a dialysis bag (cut-off molecular weight 500 Da) for 2 days. The suspension of g-C_3N_5-dots was finally obtained and stored at 4 °C for further characterization and applications.

2.5 Calculation of FLQY

The FLQY of g-C_3N_5-dots was calculated using quinine sulfate as a reference. Quinine sulfate (literature $\Phi = 0.54$) was dissolved in 0.1 M H_2SO_4, and the g-C_3N_5-dots were dispersed in ultrapure water. The QY_s was determined by comparing the integrated FL intensity and the absorbance value of the g-C_3N_5-dots samples with that of the references. The absorbance less than 0.05 (at the excitation wavelength) at 335 nm and 360 nm for quinine sulfate and g-C_3N_5-dots was obtained, respectively. The slope method was used to calculate the QY_s of g-C_3N_5-dots using the equation:

$$QY_u = QY_s(m_u/m_s)(n_u/n_s) \quad (1)$$

where QY is the quantum yield, m is the slope determined by the curves and n is the refractive index (1.33 for water and a 0.1 mol L^{-1} H_2SO_4 aqueous solution). The subscript "s" refers to the standards and "u" refers to the unknown samples. For these aqueous solution, $n_u/n_s = 1$. Series of concentrations of the references and the g-C_3N_5-dots samples were measured to obtain the slopes.

2.6 Cell imaging and toxicity assay

The cytotoxicity of the g-C_3N_5-dots to human epithelial carcinoma (Hela) cells was evaluated by a standard methylthiazolydiphenyltetrazolium bromide (MTT) assay. Hela cells were seeded in 96-well U-bottom plates at a density of approx. 5×10^4 to 1×10^5 cells per mL (90 mL per well) that were initially cultured for 12 h in an incubator (37 °C, 5% CO_2), followed by the addition of the g-C_3N_5-dots suspension with different

concentrations. After another 24 h of being cultured with the g-C_3N_5-dots, 20 mL of the MTT solution (normal saline or 1 mg mL^{-1} phosphate buffer solution) was added to each sample and incubated at 37 °C for 4 h. The culture media were discarded, followed by the addition of 150 mL of dimethyl sulfoxide (DMSO) to dissolve the formazan under shaking for more than 15 min. The cell viability rate (VR) was calculated based on the following equation:

$$\mathrm{VR}\ (\%) = A/A_0 \times 100\% \quad (2)$$

where A is the absorbance of the experimental group (the cells that were treated with the g-C_3N_5-dots suspensions) and A_0 is the absorbance of the control group.

3 Results and discussion

3.1 Characterization of the g-C_3N_5-dots

To obtain g-C_3N_5-dots with high FLQY, the effect of the mass ratio of g-C_3N_5 powder and NaOH, hydrothermal temperature, and hydrothermal time were optimized. As shown in Fig. S1,† the precursors (the mass ratio of g-C_3N_5 powder and NaOH was 0.03 : 0.3) were heated to 180 °C in an electric oven and kept for 60 min. The FL intensity of the prepared g-C_3N_5-dots reaches the highest value. Furthermore, the FLQY of as-prepared g-C_3N_5-dots was investigated at different synthesis conditions and the results are listed in (Table S2†). And the quinine sulfate solution (quantum yield 54%) was acted as reference. The highest FLQY of as-prepared g-C_3N_5-dots is 12.0%. From the above, the excellent g-C_3N_5-dots with the highest FLQY can be obtained from hydrothermal reaction of 0.03 : 0.3 g-C_3N_5/NaOH at 180 °C for 60 min and be chosen as fluorescent probes for further application.

To explore the morphology of the as-prepared g-C_3N_5-dots, we investigated their transmission electron microscopy (TEM) image, high-resolution transmission electron microscopy (HRTEM) image, X-ray diffraction (XRD) spectra. As shown in Fig. 1A, the TEM image of the g-C_3N_5-dots reveals that the as-prepared g-C_3N_5-dots are well-dispersed in water (Fig. 1A). A well-resolved crystal lattice noted in the high-resolution TEM (HRTEM) image (inset in Fig. 1A) confirms the crystalline structure of the g-C_3N_5-dots. The labeled interplanar distance is 0.24 nm, which is consistent with the (100) lattice spacing of graphene.[29,30] To further investigate the crystal structure of g-C_3N_5-dots, X-ray diffraction (XRD) patterns of bulk g-C_3N_5 and g-C_3N_5-dots were analyzed. As shown in Fig. S2,† the prepared g-C_3N_5-dots still have high crystallinity and stable crystal structure. For the bulk g-C_3N_5, the XRD patterns presents two diffraction peaks at 27.1° and 12.1°, which are attributed to the interplanar stacking of CN layers and are characteristic peaks of polymeric carbon nitride. For the g-C_3N_5-dots, the absence of the small peak at 12.1° reveals that the products display the decreased planar size of the CN layers. Meanwhile, the (002) peak shifts from 27.1° for bulk carbon nitride to 27.1°, which indicates the gallery distances are tuned during the formation process of g-C_3N_5-dots. As shown in Fig. 1B, the main diameter of g-C_3N_5-dots is about 3 nm. The result suggests that the prepared g-C_3N_5-dots have a prospect in cell imaging. In addition, we further investigated the dispersity of g-C_3N_5-dots dispersed in different organic solvents such as ethyl acetate (EA), trichloromethane ($CHCl_3$) and dimethylsulfoxide (DMSO). As shown in Fig. S3A and B,† g-C_3N_5-dots dispersed in EA and $CHCl_3$ occur agglomeration to some extent, respectively. However, g-C_3N_5-dots are well-dispersed in DMSO (Fig. S3C).† It may be because that the profuse surface hydrophilic groups (–OH, –COOH, and $–NH_2$) on the surface of g-C_3N_5-dots endow g-C_3N_5-dots with good polarity and dispersity in water and DMSO.[31]

To investigate the functional information of g-C_3N_5-dots, the Fourier transform infrared (FT-IR) spectra of g-C_3N_5-dots were obtained. We explored the FTIR spectrum of bulk g-C_3N_5 firstly. As shown in Fig. 2A, the FTIR spectrum for bulk g-C_3N_5 shows a peak at 3136 cm^{-1} which corresponds to the stretching vibrations of $–NH_2$.[32] The region between 1670 and 1500 cm^{-1} is related to all the feature distinctive stretch modes of aromatic CN heterocycles that is the stretching vibrations of C=O and C–N.[33,34] The peak at 1428 cm^{-1} is attributed to the ring breathing modes of triazole ring.[35] The strong bands in 1000–700 cm^{-1} region are assigned to out-of-plane bending vibrations of N–H.[36,37] Compared with the FT-IR spectrum of bulk g-C_3N_5, the

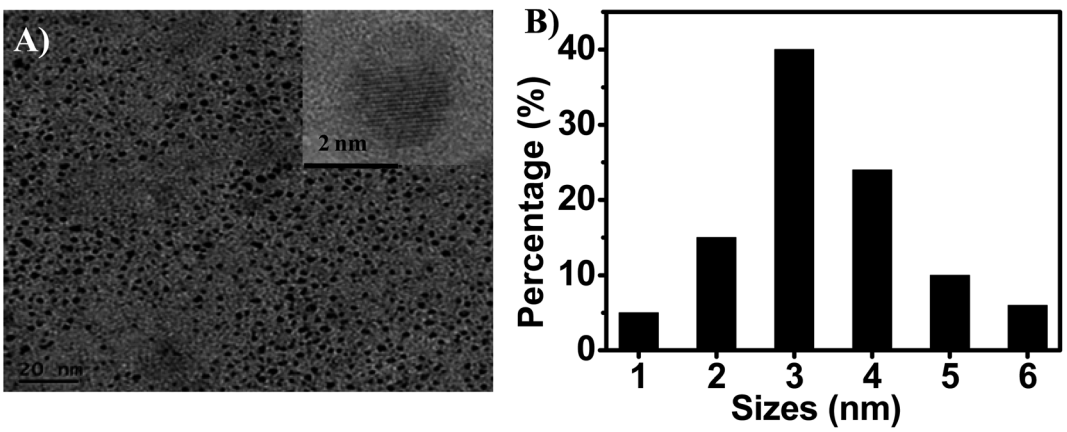

Fig. 1 (A) Typical TEM and HRTEM (inset) images of g-C_3N_5-dots. (B) Size distribution histograms of g-C_3N_5-dots.

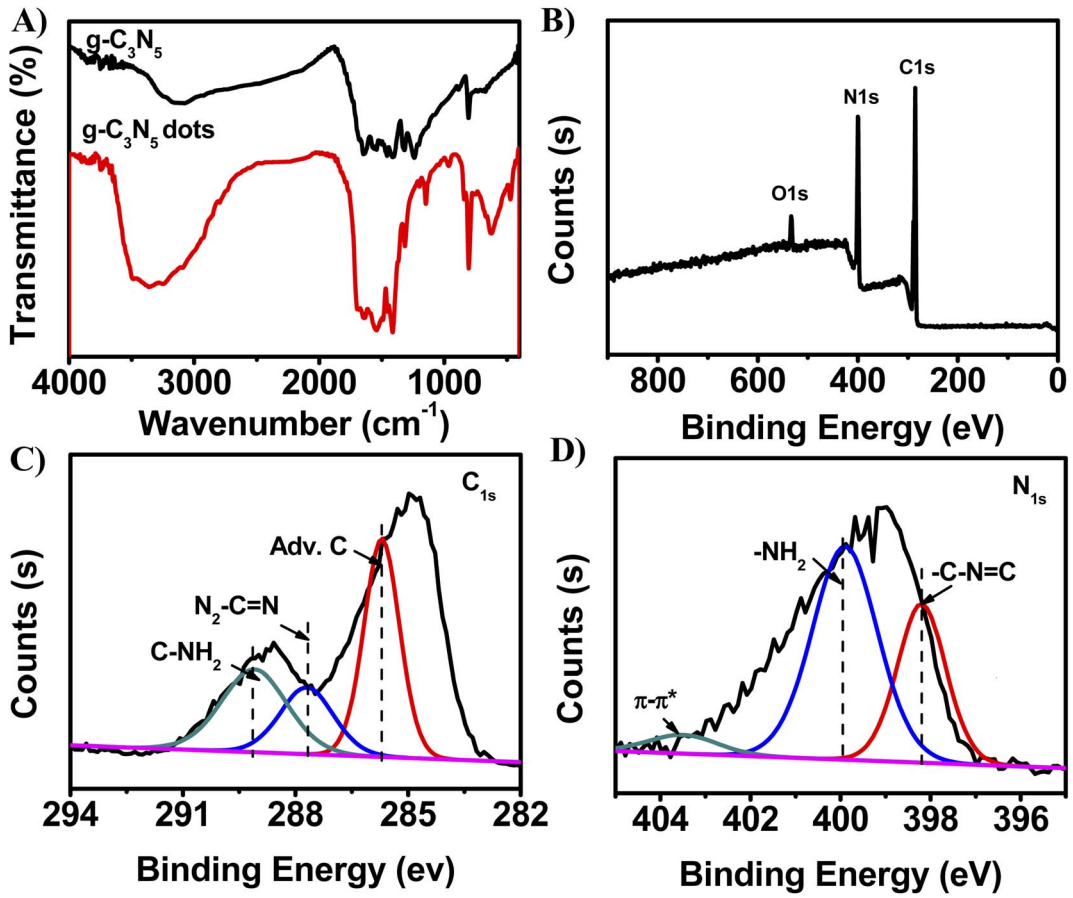

Fig. 2 (A) FT-IR spectra of g-C_3N_5-dots after hydrothermal treatment of 0.03 g g-C_3N_5 powder with 0.3 g NaOH under 180 °C for 1 h. (B) XPS full spectra of g-C_3N_5-dots. High-resolution XPS of (C) C_{1s} and (D) N_{1s} of g-C_3N_5-dots prepared by hydrothermal treatment of 0.03 g g-C_3N_5 powder with 0.3 g NaOH under 180 °C for 60 min.

peaks of products are almost no change after alkaline assisted-hydrothermal process. The result indicates that g-C_3N_5-dots preserve the same functional structure as bulk g-C_3N_5. However, the FT-IR spectrum of g-C_3N_5-dots shows a new and strong peak at 3380 cm^{-1}, which is attributed to the bending vibrations of –OH.[31] We infer that –OH is generated by breaking the structure of bulk g-C_3N_5 in the process of alkaline assisted hydrothermal treatment. These above results confirm that the as-synthesized nanoparticles are functionalized by –OH and –COOH.

On the other hand, we further investigated functional information of g-C_3N_5-dots *via* X-ray photoelectron spectra (XPS). The XPS survey spectrum (Fig. 2B) of g-C_3N_5-dots further confirms that the material is mainly composed of 36.44% C and 61.8% N with 1.76% O. The small amount of O can be related to CO_2 adsorption on the surface of g-C_3N_5-dots.[35] The C_{1s} spectra (Fig. 2C) suggest that the presence of C–NH_2 (289.1 eV), N_2–C=N (287.7 eV) and adventitious C (285.7 eV).[38–40] The N_{1s} spectra (Fig. 2D) show three peaks at 403.5 eV, 399.9 eV, and 398.2 eV, which are attributed to the π–π*, –C–NH_2, and –C–N=C, respectively.[41,42] π–π* and –C–N=C reveal the presence of graphitic sp^2 network. And –C–NH_2 further confirm that the presence of tris-triazine ring in the CN framework.[43]

3.2 The synthetic mechanism of g-C_3N_5-dots

Additionally, the possible synthetic mechanism of g-C_3N_5-dots was proposed. Under alkaline assisted-hydrothermal condition, the hydroxyl groups can be transferred to produce free radicals (*e.g.* $^{\bullet}OH$ and $^{\bullet}O^{-}$).[44] These free radicals are the key for the cleavage of bulk g-C_3N_5 into small g-C_3N_5-dots in the hydrothermal process under alkaline solution. To demonstrate our inference, g-C_3N_5 powder was treated by hydrothermal strategy under neutral (pure water) solution, acid solution (1.5 M HCl) and alkaline solution (1.5 M NaOH) for 60 min, respectively. And the morphology features, optical properties and functional information of these obtained products were characterized. Firstly, the TEM images of the synthesized products were obtained to study the effect of different solution conditions on the morphology of the prepared products, respectively. As shown in Fig. S4,† the products prepared by hydrothermal method with the treatment of neutral solution and HCl solution display bulk structure with large size, respectively. However, the product prepared by alkaline assisted-hydrothermal method uniformly distribute in water and the diameters of g-C_3N_5-dots mainly distribute in the range of 2–4 nm. The result is due to the fact that the free radicals obtained from alkaline assisted-hydrothermal condition can break C–N bonds on the g-C_3N_5

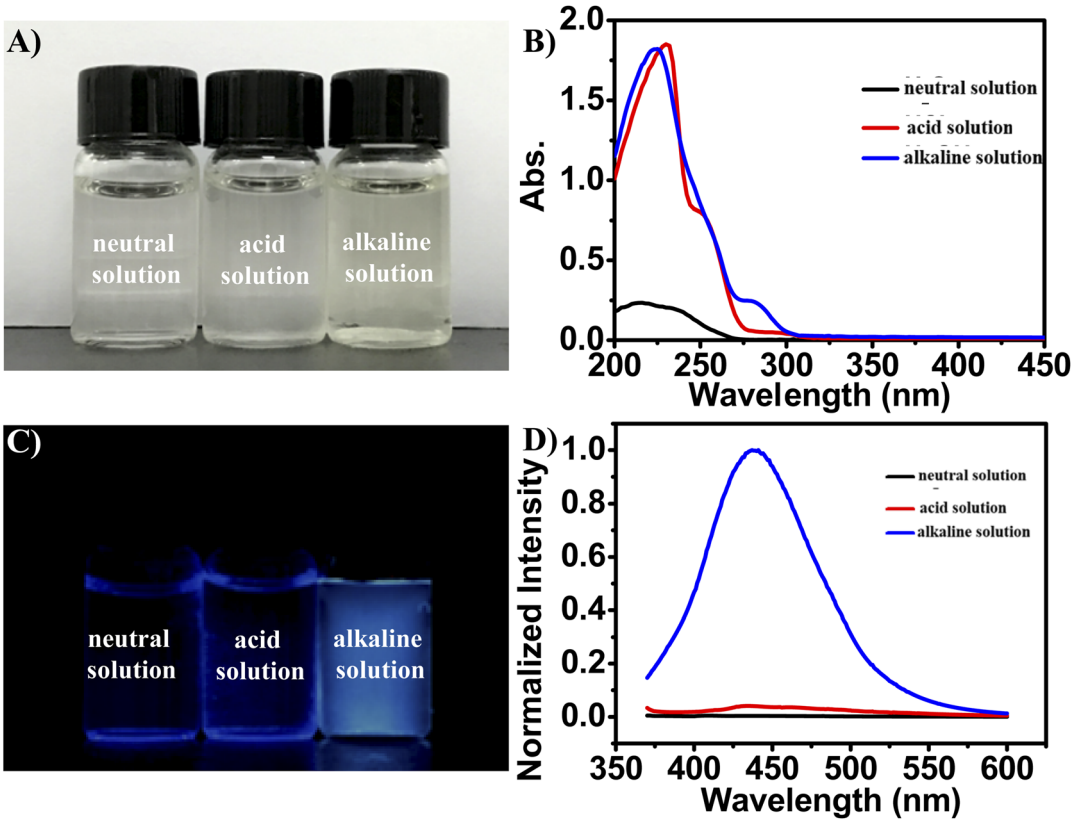

Fig. 3 The (A) day light and (C) 365 nm UV light irradiation photographs of synthesized products under different conditions (neutral solution, acid solution and alkaline solution), and corresponding (B) UV-vis and (D) FL spectra, respectively. The aqueous solutions are without dilution or enrichment, the excitation wavelength of is 360 nm.

framework. These free radicals acting as "scissors" cut large-sized g-C_3N_5 fragments into g-C_3N_5-dots. Furthermore, the alkaline assisted-hydrothermal process for synthesis of g-C_3N_5-dots was investigated by TEM. From Fig. S5,† it is noted that the product obtained from alkaline assisted-hydrothermal process at 30 min has a larger size (12 nm) compared with the product obtained at 60 min (3 nm). Based on above discussion, the larger-sized g-C_3N_5 is cut into smaller-sized g-C_3N_5, and then is converted into g-C_3N_5-dots finally. And the alkali environment facilitates the formation of g-C_3N_5-dots.

Secondly, UV-vis spectra and fluorescence spectra of their products were explored to investigate the effect of solution condition on optical properties of the obtained products. As shown in Fig. 3A, the day light photographs of synthesized products under neutral solution and acid solution show colorless clear, respectively. However, the day light photograph of synthesized product under alkaline solution shows light yellow and the product show two obvious absorbance peaks at 225 nm and 280 nm (Fig. 3B). And the control experiments (Fig. 3C and D) show that products in neutral and acid environments have no FL, whereas the product obtained from alkaline assisted-hydrothermal condition exhibits distinct FL under excitation. That is because bulk g-C_3N_5 is cut by the radical species into g-C_3N_5-dots. The quantum dots with sizes less than 10 nm have excellent optical properties due to their quantum confinement effect.

Thirdly, XPS spectra of three prepared products in different conditions were explored to further investigate the effects of synthetic conditions on the functional information of products. As shown in Fig. 4A and B, high-resolution XPS of the C_{1s} and N_{1s} of three prepared products have little change. And the peak area of $-NH_2$, –C–N=C, C–NH_2, N_2–C=N and Adv. C almost remain unchanged (Table 1). However, the peak area of both C–OH and C=O of the product obtained from alkaline assisted-hydrothermal condition is larger than that of the products in neutral and acid environments (Fig. 4A and Table 1). The result is consistent with UV-vis spectra (Fig. 3B). Based on the above discussion, we infer that alkaline condition makes for the production of –OH and C=O. And the abundant electron donor groups (–OH and $-NH_2$) on the surface of g-C_3N_5-dots obtained from alkaline assisted-hydrothermal process are beneficial to fluorescence emission.

It is noted that optical property is an important parameter to their future application in biosensors and bioimaging. Therefore, the optical properties of g-C_3N_5-dots were characterized by ultraviolet-visible (UV-vis) spectrophotometer and FL spectrophotometer. As shown in Fig. 5A, the characteristic absorption peaks around 225 nm and 280 nm found in the UV-vis spectra are ascribed to the n–π* transition of C=O and π–π* transition of C=C, respectively.[45] The as-synthesized g-C_3N_5-dots have a maximum emission at 440 nm under an excitation at 360 nm (Fig. 5A). FL emission spectra of g-C_3N_5-dots display excitation-

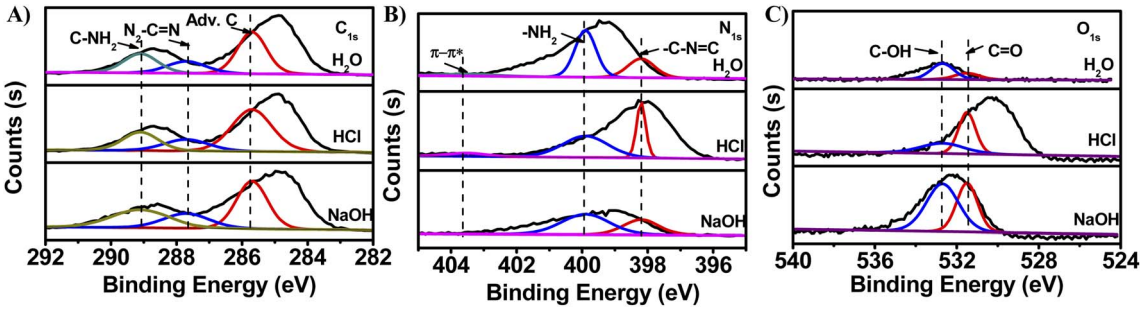

Fig. 4 High-resolution XPS of (A) C_{1s}, (B) N_{1s} and (C) O_{1s} of synthesized products under different conditions (H_2O, 1.5 M HCl and 1.5 M NaOH), respectively.

Table 1 Peak area of binding energy of high-resolution XPS data of O_{1s}, N_{1s} and C_{1s} of synthesized products under different conditions (H_2O, 1.5 M HCl and 1.5 M NaOH), respectively

	Peak area (O_{1s})		Peak area (N_{1s})		Peak area (C_{1s})		
Different conditions	C–OH	C=O	$-NH_2$	–C–N=C	C–NH_2	N_2–C=N	Adv. C
H_2O	2816.32	1210.31	7587.91	3970.94	6779.36	4459.06	9715.36
HCl	3034.85	4802.70	7360.12	4101.93	6230.16	4906.48	12 099.17
NaOH	10 124.06	8953.22	7360.12	3875.86	6267.98	4481	11 591.41

dependent FL behavior at different excitation wavelengths that change from 320 nm to 460 nm. This behavior is attributed to surface defect and size distribution of g-C_3N_5-dots.[46–48] The FLQY of the prepared g-C_3N_5-dots is calculated with quinine sulfate solution (quantum yield of 54%) as reference (Fig. S6†).[49,50] The fluorescence quantum yield (FLQY) of the prepared g-C_3N_5-dots is calculated to be about 12%. And we choose the optimum g-C_3N_5-dots with a high FLQY for further application.

3.3 The optical stability of g-C_3N_5-dots

To explore the optical stability of g-C_3N_5-dots, a detailed FL study was obtained. The FL intensities of g-C_3N_5-dots have little change even under high salt concentration (Fig. S7A).† And the FL intensities of g-C_3N_5-dots are pH independent under acidic or basic conditions (Fig. S7B).† As mentioned above, as-synthesized g-C_3N_5-dots are functionalized by abundant oxygen-containing functional groups (such as –OH and –COOH), which improve the hydrophilicity and stability of them in aqueous. What is more, the FL intensity does not change even after continuous excitation with a 150 W Xe lamp (Fig. S7C).† Otherwise, the FL intensities of g-C_3N_5-dots are stable for more than a month without any distinct reduction (Fig. S7D).† The results demonstrate that the as-synthesized g-C_3N_5-dots have excellent photostability. According to these unique optical properties of g-C_3N_5-dots, g-C_3N_5-dots have tremendous practical application potential in the field of biosensors and bioimaging.

3.4 The bioimaging and peroxidase-like activity of g-C_3N_5-dots

Compared with bulk g-C_3N_5 materials, their quantum dots exhibit distinct physicochemical properties due to their quantum confinement effect. Therefore, it is possible to expand the potential application in bioimaging of g-C_3N_5-dots. Firstly, the cytotoxicity of the g-C_3N_5-dots was investigated by the 3-(4,5-

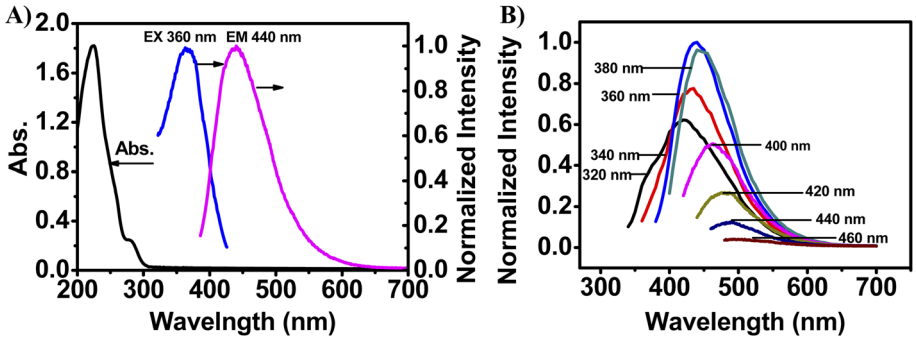

Fig. 5 (A) UV-vis spectra and fluorescence spectra of g-C_3N_5-dots. (B) Fluorescence emission spectra of g-C_3N_5-dots at different excitation wavelengths that change from 320 nm to 460 nm.

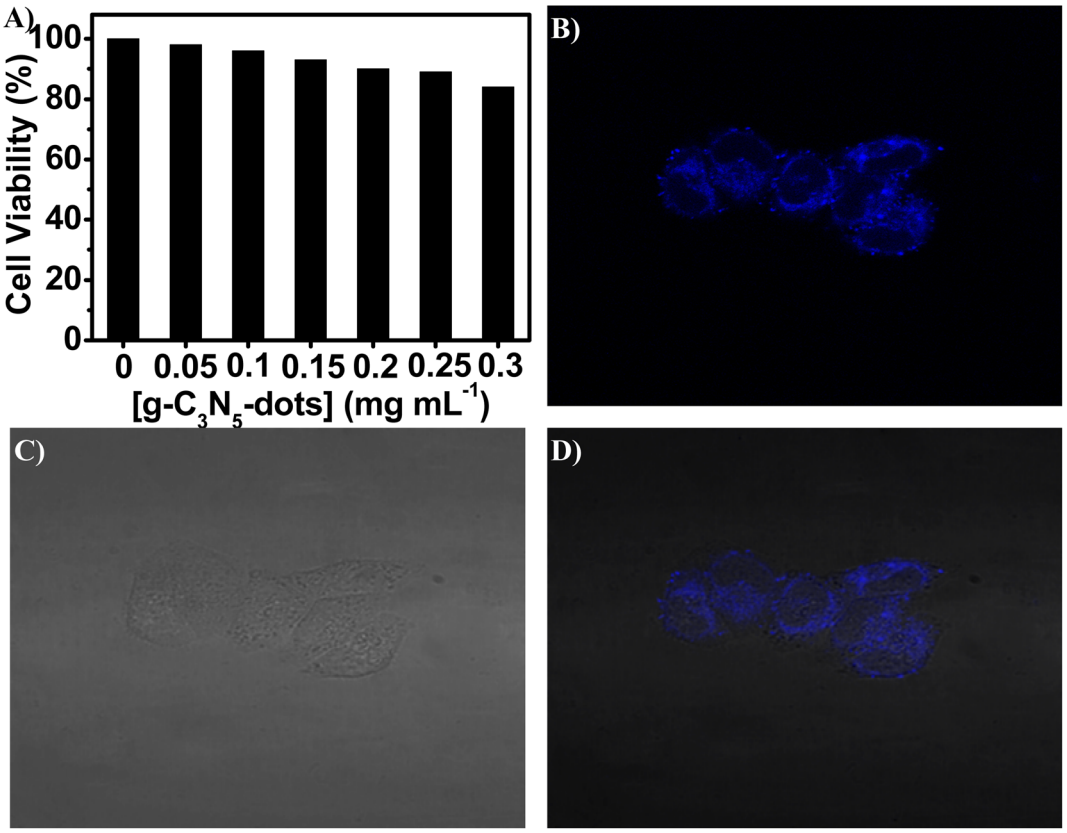

Fig. 6 (A) Cell viability assay of C_3N_5-dots at different concentrations. (B and C) Confocal fluorescent images of g-C_3N_5-dots in HeLa cells. (B) The image excited with 405 nm laser and (C) their corresponding bright-field images of Hela cells. (D) The overlay of bright-field and fluorescence images. The concentration of g-C_3N_5-dots is 0.15 mg mL^{-1}.

dimethylthiazol-2-yl)-2,5-diphenyltetrazolium bromide (MTT) assay. From Fig. 6A, the result shows that the cell viability remains greater than 86% with the increasing concentration of g-C_3N_5-dots in the range of 0.05–0.3 mg mL^{-1}. The result indicates that the g-C_3N_5-dots have low cytotoxicity and excellent biocompatibility. Then, the g-C_3N_5-dots were introduced into HeLa cells for *in vitro* bioimaging. As shown in Fig. 6B, the HeLa cells display good morphology. And a significant blue emission from the intracellular region could be observed in dark field. From Fig. 6C and D, the cell morphology displays no significant changes. All these results indicate that the as-synthesized g-C_3N_5-dots exhibit low cytotoxicity and excellent biocompatibility and have the application potentials as FL probe for bioimaging and related biological applications.

Additionally, we investigated the peroxidase-like activity of g-C_3N_5-dots in the catalysis for oxidation of peroxidase substrates TMB (or OPD) in presence of H_2O_2. As shown in Fig. S8,† TMB–H_2O_2, TMB–g-C_3N_5-dots, OPD–H_2O_2, OPD–g-C_3N_5-dots systems have no absorbance peak and their solutions exhibit colorless. However, there are two obvious absorbance peaks at 652 nm and 444 nm in TMB–g-C_3N_5-dots–H_2O_2 system and OPD–g-C_3N_5-dots–H_2O_2 system, respectively. Up to now, there are few reports about g-C_3N_5-dots as enzymatic mimetics. The peroxidase-like activity of g-C_3N_5-dots is similar to the reported other quantum dots.[51] These results suggest that the as-prepared g-C_3N_5-dots possess excellent peroxidase-like activity, further indicating the tremendous practical application potential in the field of biosensors.

4 Conclusion

In summary, the novel g-C_3N_5-dots were fabricated by a facile alkaline-assisted hydrothermal strategy for the first time. The synthetic mechanism of g-C_3N_5-dots was discussed. Under the alkaline-assisted hydrothermal process, the high temperature and high pressure conditions make hydroxyl groups transfer to produce free radicals. These free radicals acting as "scissors" cut large-sized g-C_3N_5 fragments into g-C_3N_5-dots. The proposed method has many advantages of low-cost, easy operation and time-saving. The entire synthetic process of high fluorescence g-C_3N_5-dots requires only 60 min. The as-prepared g-C_3N_5-dots with triazole ring display superior salt tolerance, pH-stability, anti-photobleaching and excitation-dependent behavior. In addition, g-C_3N_5-dots with low toxicity and excellent biocompatibility were successfully used for cell imaging. The study provides a simple and effective strategy for synthesis of g-C_3N_5-dots and prompts the novel g-C_3N_5-dots for some potential application in the field of biosensors and bioimaging.

Conflicts of interest

There are no conflicts to declare.

Acknowledgements

The work was financially supported by National Natural Science Foundation of China (21964006, 52173034, 51973056), the Hunan Provincial Natural Science Foundation of China (2021JJ50009, 2020JJ4640, 2020JJ5348), the Science and Technology Innovation Program of Hunan Province (2021RC4065), the Scientific Research Fund of Hunan Provincial Education Department (18A258, 20A050, 21B0764), the Changsha Science and Technology Planning Project (kq2203003) and the Scientific Research Found of Changsha University (SF1954), respectively.

References

1 J. Liu, R. Li and B. Yang, *ACS Cent. Sci.*, 2020, **6**, 2179–2195.
2 J. Yao, M. Yang and Y. Duan, *Chem. Rev.*, 2014, **114**, 6130–6178.
3 Y. Wang, K. Lu, L. Han, Z. Liu, G. Shi, H. Fang, S. Chen, T. Wu, F. Yang, M. Gu, S. Zhou, X. Ling, X. Tang, J. Zheng, A. Loi Maria and W. Ma, *Adv. Mater.*, 2018, **30**, 1704871–1704878.
4 Y. Zhao, L. Tan, X. Gao, G. Jie and T. Huang, *Biosens. Bioelectron.*, 2018, **110**, 239–245.
5 X. Pan, Y. Dong, M. Jia, J. Wen, C. Su, Y. Shang, X. Zhang, F. Pang and T. Wang, *Appl. Surf. Sci.*, 2021, **546**, 149086.
6 Y. Ma Tian, J. Ran, S. Dai, M. Jaroniec and Z. Qiao Shi, *Angew. Chem., Int. Ed.*, 2014, **54**, 4646–4650.
7 P. Xia, B. Zhu, J. Yu, S. Cao and M. Jaroniec, *J. Mater. Chem. A*, 2017, **5**, 3230–3238.
8 S. Zhao, Y. Zhang, Y. Zhou, Y. Wang, K. Qiu, C. Zhang, J. Fang and X. Sheng, *Carbon*, 2018, **126**, 247–256.
9 B.-R. Wulan, S.-S. Yi, S.-J. Li, Y.-X. Duan, J.-M. Yan and Q. Jiang, *Appl. Catal., B*, 2018, **231**, 43–50.
10 J. Wang and S. Wang, *Coord. Chem. Rev.*, 2022, **453**, 214338.
11 Y. Gong, X. Zhao, H. Zhang, B. Yang, K. Xiao, T. Guo, J. Zhang, H. Shao, Y. Wang and G. Yu, *Appl. Catal., B*, 2018, **233**, 35–45.
12 J. Oh, Y. Shim, S. Lee, S. Park, D. Jang, Y. Shin, S. Ohn, J. Kim and S. Park, *J. Solid State Chem.*, 2018, **258**, 559–565.
13 Q. Liu, T. Chen, Y. Guo, Z. Zhang and X. Fang, *Appl. Catal., B*, 2016, **193**, 248–258.
14 P. Yan, D. Jiang, Y. Tian, L. Xu, J. Qian, H. Li, J. Xia and H. Li, *Biosens. Bioelectron.*, 2018, **111**, 74–81.
15 D. Zhu, S. Liu, M. Chen, J. Zhang and X. Wang, *Colloids Surf., A*, 2018, **537**, 372–382.
16 F. Wang, Y. Feng, P. Chen, Y. Wang, Y. Su, Q. Zhang, Y. Zeng, Z. Xie, H. Liu, Y. Liu, W. Lv and G. Liu, *Appl. Catal., B*, 2018, **227**, 114–122.
17 B. Hu, Y. Liu, Z.-W. Wang, Y. Song, M. Wang, Z. Zhang and C.-S. Liu, *Appl. Surf. Sci.*, 2018, **441**, 694–707.
18 J. Zhu, W. Nie, Q. Wang, J. Li, H. Li, W. Wen, T. Bao, H. Xiong, X. Zhang and S. Wang, *Carbon*, 2018, **129**, 29–37.
19 P. Mane Gurudas, N. Talapaneni Siddulu, S. Lakhi Kripal, H. Ilbeygi, U. Ravon, K. Al-Bahily, T. Mori, D.-H. Park and A. Vinu, *Angew. Chem., Int. Ed.*, 2017, **56**, 8481–8485.
20 C. Hu, Y.-H. Lin, M. Yoshida and S. Ashimura, *ACS Appl. Mater. Interfaces*, 2021, **13**, 24907–24915.
21 H. Wang, M. Li, Q. Lu, Y. Cen, Y. Zhang and S. Yao, *ACS Sustainable Chem. Eng.*, 2019, **7**, 625–631.
22 F. Nemati, A. B. Pebdeni and M. Hosseini, in *Biosensor Based Advanced Cancer Diagnostics*, eds. R. Khan, A. Parihar and S. K. Sanghi, Academic Press, 2022, 225–243.
23 M. Bacon, J. Bradley Siobhan and T. Nann, *Part. Part. Syst. Charact.*, 2013, **31**, 415–428.
24 J. Peng, W. Gao, B. K. Gupta, Z. Liu, R. Romero-Aburto, L. Ge, L. Song, L. B. Alemany, X. Zhan, G. Gao, S. A. Vithayathil, B. A. Kaipparettu, A. A. Marti, T. Hayashi, J.-J. Zhu and P. M. Ajayan, *Nano Lett.*, 2012, **12**, 844–849.
25 M. Bacon, S. J. Bradley and T. Nann, *Part. Part. Syst. Charact.*, 2014, **31**, 415–428.
26 J. Duan, Y. Zhang, Y. Yin, H. Li, J. Wang and L. Zhu, *Sens. Actuators, B*, 2018, **257**, 504–510.
27 Q. Liu, X. Wang, Q. Yang, Z. Zhang and X. Fang, *Appl. Catal., B*, 2018, **225**, 22–29.
28 A. Hatamie, F. Marahel and A. Sharifat, *Talanta*, 2018, **176**, 518–525.
29 L. C. Sim, J. L. Wong, C. H. Hak, J. Y. Tai, K. H. Leong and P. Saravanan, *Beilstein J. Nanotechnol.*, 2018, **9**, 353–363.
30 L. Tang, R. Ji, X. Cao, J. Lin, H. Jiang, X. Li, K. S. Teng, C. M. Luk, S. Zeng, J. Hao and S. P. Lau, *ACS Nano*, 2012, **6**, 5102–5110.
31 J. Deng, Q. Lu, N. Mi, H. Li, M. Liu, M. Xu, L. Tan, Q. Xie, Y. Zhang and S. Yao, *Chem.–Eur. J.*, 2014, **20**, 4993–4999.
32 H. Wang, Q. Lu, Y. Hou, Y. Liu and Y. Zhang, *Talanta*, 2016, **155**, 62–69.
33 J. Liu, J. Huang, H. Zhou and M. Antonietti, *ACS Appl. Mater. Interfaces*, 2014, **6**, 8434–8440.
34 Q. Cui, J. Xu, X. Wang, L. Li, M. Antonietti and M. Shalom, *Angew. Chem., Int. Ed.*, 2016, **55**, 3672–3676.
35 G. P. Mane, S. N. Talapaneni, K. S. Lakhi, H. Ilbeygi, U. Ravon, K. Al-Bahily, T. Mori, D.-H. Park and A. Vinu, *Angew. Chem., Int. Ed.*, 2017, **56**, 8481–8485.
36 X. M. Lin Zhu, N. Liu, G. Xu and C. Huang, *Acta Phys. -Chim. Sin.*, 2016, **32**, 2488–2494.
37 H. Wang, Q. Lu, M. Li, H. Li, Y. Liu, H. Li, Y. Zhang and S. Yao, *Anal. Chim. Acta*, 2018, **1027**, 121–129.
38 K. Patir and S. K. Gogoi, *ACS Sustainable Chem. Eng.*, 2018, **6**, 1732–1743.
39 Z. Chen, X. Yu, Q. Zhu, T. Fan, Q. Wu, L. Zhang, J. Li, W. Fang and X. Yi, *Carbon*, 2018, **139**, 189–194.
40 C. P. Ewels and M. Glerup, *J. Nanosci. Nanotechnol.*, 2005, **5**, 1345–1363.
41 D. Dontsova, S. Pronkin, M. Wehle, Z. Chen, C. Fettkenhauer, G. Clavel and M. Antonietti, *Chem. Mater.*, 2015, **27**, 5170–5179.
42 H. Yuan, J. Liu, H. Li, Y. Li, X. Liu, D. Shi, Q. Wu and Q. Jiao, *J. Mater. Chem. A*, 2018, **6**, 5603–5607.
43 E. Lieber, C. N. R. Rao, C. N. Pillai, J. Ramachandran and R. D. Hites, *Can. J. Chem.*, 1958, **36**, 801–809.
44 J. Deng, Q. Lu, H. Li, Y. Zhang and S. Yao, *RSC Adv.*, 2015, **5**, 29704–29707.
45 X. Yan, Y. Song, C. Zhu, H. Li, D. Du, X. Su and Y. Lin, *Anal. Chem.*, 2017, **90**, 2618–2624.

46 H. Wang, Q. Lu, Y. Liu, H. Li, Y. Zhang and S. Yao, *Sens. Actuators, B*, 2017, **250**, 429–435.
47 W. Yang, J. Ni, F. Luo, W. Weng, Q. Wei, Z. Lin and G. Chen, *Anal. Chem.*, 2017, **89**, 8384–8390.
48 M. Kaur, S. K. Mehta and S. K. Kansal, *Sens. Actuators, B*, 2017, **245**, 938–945.
49 F. Niu, Y.-L. Ying, X. Hua, Y. Niu, Y. Xu and Y.-T. Long, *Carbon*, 2018, **127**, 340–348.
50 B.-P. Jiang, Y.-X. Yu, X.-L. Guo, Z.-Y. Ding, B. Zhou, H. Liang and X.-C. Shen, *Carbon*, 2018, **128**, 12–20.
51 Q. Chen, M. Liu, J. Zhao, X. Peng, X. Chen, N. Mi, B. Yin, H. Li, Y. Zhang and S. Yao, *Chem. Commun.*, 2014, **50**, 6771–6774.